Machine Learning based Condition Monitoring for SiC MOSFETs in Hydrokinetic Turbine Systems

Alastair P. Thurlbeck, Student Member, IEEE
School of Electrical Engineering and Computer Science
Oregon State University
Corvallis, Oregon 97331
Email: thurlbea@oregonstate.edu

Yue Cao, Member, IEEE
School of Electrical Engineering and Computer Science
Oregon State University
Corvallis, Oregon 97331
Email: yue.cao@oregonstate.edu

***Abstract*—This work demonstrates a machine learning (ML) based condition monitoring system for silicon carbide MOSFETs in a hydrokinetic turbine (HKT) energy conversion system. In this application, the power electronics are underwater, and their maintenance is challenging and expensive. At the device level, MOSFET on-state resistance (R_{dson}) can be monitored to track MOSFET degradation. Conventionally, the variation in R_{dson} with temperature is compensated for by explicit measurement or estimation of junction temperature T_J, which can be difficult to implement. Instead, in the proposed system, R_{dson} load and temperature dependencies are accounted for via a ML model of the system, which first predicts the R_{dson} of a healthy MOSFET given the system operating conditions, and then this prediction of healthy R_{dson} is compared to the actual R_{dson} measurement, with the difference tracking the change in R_{dson} due to degradation. This ML based method is particularly advantageous for the HKT system, since the dynamics of the electrical and thermal systems as well as their variation with water speed or temperature do not need to be modeled. The proposed condition monitoring (CM) systems using this ML approach are demonstrated by simulation and experimental testing.**

***Index Terms*—Turbines, Hydrokinetic energy, Power conversion, Power electronics, Machine Learning, Condition monitoring.**

I. Introduction

The hydrokinetic turbine (HKT) system comprises of a submerged turbine in a riverine environment, a permanent-magnet synchronous generator (PMSG), a fully rated back-to-back power electronic converter, and an LCL filter. Whilst the electrical topology and controls are comparable to a direct-drive wind turbine system, the thermal dynamics of the electrical system are unique. Assuming the power electronics are also submerged in the river, the heat transfer mechanism from the enclosure to the water is mostly forced convection, varying with water velocity and temperature. Silicon carbide (SiC) MOSFETs are an attractive switching device for the HKT system owing to their higher breakdown voltage, faster switching transitions, and reduced R_{dson} compared to traditional silicon switching devices. To optimize maintenance and improve the converter system reliability, converter MOSFET degradation can be monitored. This device-level condition monitoring (CM) can provide an estimate of remaining useful life of the converter, or can be used for failure prognosis. In either case, CM can help reduce the high operating costs of the HKT system via condition-based maintenance, and the availability of the HKT system can be improved by replacing a degraded part before it fails completely.

Device failures are either extrinsic or intrinsic. Extrinsic failures relate to the device packaging, whereas intrinsic failures occur within the die itself. SiC MOSFETs appear particularly susceptible to dielectric breakdown, caused by high temperatures and high electric fields across the gate oxide layer. This is in contrast to devices such as IGBTs and silicon MOSFETs, where packaging failures such as solder joint cracking or wire bond liftoff are the dominant failure mechanisms [1], [2]. Accordingly, researchers have investigated suitable failure precursors for SiC MOSFETs, which can track dielectric breakdown in addition to packaging failures. Commonly proposed precursors include threshold voltage, R_{dson}, body diode forward voltage, drain-source leakage current, and gate leakage current [3], [4]. Monitoring R_{dson} is the focus of this work, since it is feasible to measure in-situ and increases with both packaging and gate oxide degradation [3]. However, MOSFET R_{dson} depends on load and temperature. Hence MOSFET drain current I_D and junction temperature T_J must be compensated for before a change in measured R_{dson} is attributed to degradation. Whilst I_D is easily measured, T_J requires indirect measurement or estimation.

One solution is to measure MOSFET case temperature, and then estimate T_J by considering the MOSFET's power loss and junction-case thermal resistance [3]. However, accurate case temperature measurements for each converter MOSFET would have a high implementation cost. Alternatively, T_J can be estimated using a thermally sensitive electrical parameter (TSEP) [5]. Indeed, R_{dson} is a commonly used TSEP for T_J monitoring. However, R_{dson} cannot be used

This work was supported in part by the U.S. Department of Energy Advanced Research Projects Agency-Energy (ARPA-E) Award under Grant DE-AR0001438.

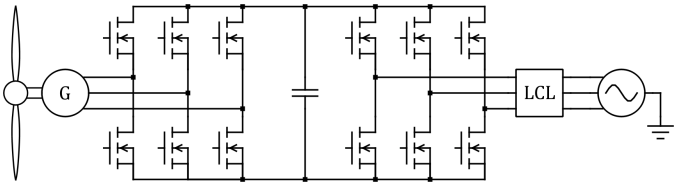

Fig. 1. HKT electrical system overview.

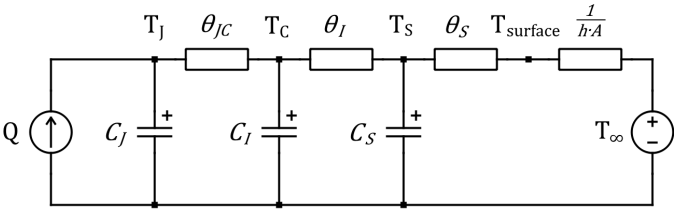

Fig. 2. MOSFET thermal equivalent circuit model.

to simultaneously estimate T_J and degradation. Other TSEPs such as threshold voltage, turn-on delay, or turn-off delay are challenging to measure, and the use of a TSEP for T_J estimation would require significant additional circuitry for each converter MOSFET.

In this paper, the proposed machine learning (ML) based CM system offers an alternative method to account for T_J in which these additional measurements at each MOSFET are not required. Instead, T_J is implicitly accounted for by training ML models to predict the R_{dson} of a healthy MOSFET over the full operating space of the HKT system. These are 'black-box' models, which map a set of measurements to the R_{dson} prediction without requiring any knowledge of the system parameters or dynamics. When degradation occurs, the ML models still predict R_{dson} as though the MOSFET is in the beginning-of-life (BOL) condition, even when the MOSFET has degraded. This prediction is then compared to the degraded MOSFET's R_{dson} measurement, with the difference tracking degradation independently of I_D and T_J.

II. Proposed ML Based CM Systems

An overview of the HKT system is shown in Fig. 1. The hydrokinetic turbine drives a PMSG, which is connected via a back-to-back AC-DC-AC power-electronic converter to the grid. Fig. 2 shows the thermal equivalent circuit model for the power-electronic converter MOSFETs. Q is the MOSFET power loss or heat transfer, h is the convective heat transfer coefficient, and A is the heatsink surface area. T_J, T_C, T_S, and $T_{surface}$ are the junction, case, heatsink, and heatsink surface temperatures, respectively. T_∞ is the water temperature beyond the thermal boundary layer. θ_{JC}, θ_I, θ_S and C_J, C_I, C_S are the junction-case, interface, and heatsink thermal resistances and capacitances, respectively. Note that θ_S represents the conductive heat transfer across the heatsink material, whereas $1/(hA)$ represents the convective heat transfer from the heatsink surface to the water. Therefore, T_J is dependent on power loss, water temperature, and the conductive and forced convection heat transfer mechanisms. These dynamics are especially pronounced in the HKT application, since power loss Q and the convective heat transfer coefficient h have strong non-linear variations with water velocity. An advantage of the proposed ML based CM system is that these complex behaviors do not need to be modeled.

Fig. 3 shows two proposed CM systems, each leveraging ML models to predict MOSFET R_{dson}. This prediction is compared to the actual measurement of R_{dson} to generate an error signal, which tracks any increase in R_{dson} due to MOSFET degradation. The more complex Fig. 3(a) system is investigated via simulation while the simplified system of Fig. 3(b) is used for experimental testing. This simplified system is used for the experimental testing since the ambient temperature could not easily be controlled, and MOSFET power loss Q would need to be experimentally measured in order to train ML Model 1 in Fig. 3(a). However, note that the overall principle of both systems is the same. Indeed, the actual implementation of the ML models is flexible, and can be tailored to the available system measurements and application. The ML models are realized in Python 3 using *pandas*, *scikit-learn*, and *TensorFlow* and *Keras* libraries. Once the models have been trained and tested offline in Python, then they can be deployed in real-time for system CM.

Considering Fig. 3(a) first, ML Model 1 predicts MOSFET power loss from the converter current magnitude, DC bus voltage, and water temperature and velocity. Then ML Model 2 predicts MOSFET R_{dson} from measured I_D, the predicted power loss from ML Model 1, and water temperature and velocity. Model 1 uses ridge regression with 4th order polynomial features [6]. The training uses a linear least squares fit loss function with L2-norm regularization. Model 2 uses an artificial neural network (ANN) [7] with four hidden layers, with sizes of: 32; 16; 16; and 8 neurons. Each neuronuses a rectified linear unit (RELU) non-linear activation function. The model is trained using an Adam optimization algorithm [8], which is an extension of the stochastic gradient descent method. Now considering Fig. 3(b), the ML model predicted MOSFET R_{dson} from measured I_D, the converter current magnitude, and the water velocity. The model uses ridge regression with 5th order polynomial features and is trained using the linear least squares fit loss function with L2-norm regularization.

By training the ML models over the full range of expected river water temperatures and velocities, the models learn the relationships between I_D and T_J and the observed R_{dson}. The measured R_{dson} value is compared to the predicted value to generate an error signal which tracks the increase in R_{dson} due to degradation only. In Fig. 3(a), the error signal gives the % change from BOL R_{dson}, while in Fig. 3(b) the error signal is the absolute change from BOL R_{dson}. If the real system is in the BOL condition, the error signals should be zero. When a MOSFET degrades, the measurement of R_{dson} will be higher than the predicted R_{dson}, and therefore the error signal should track the increase in R_{dson}.

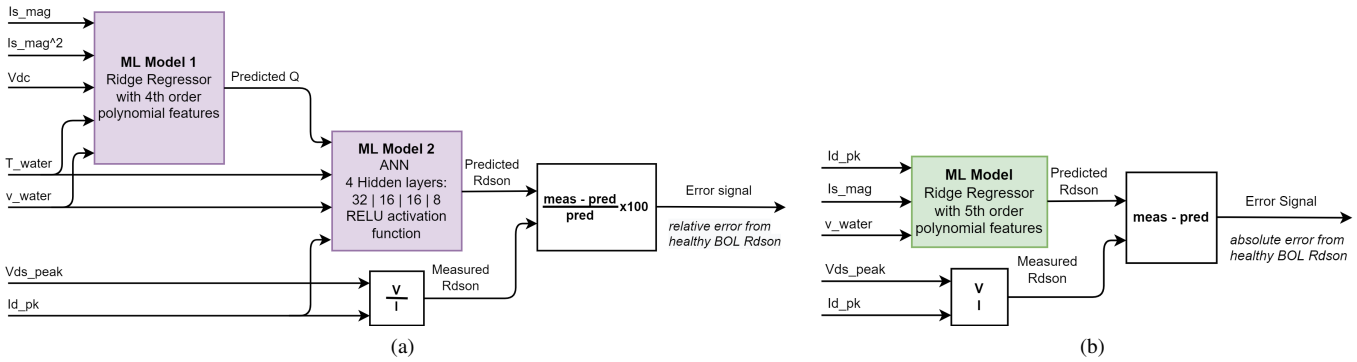

Fig. 3. Overview of proposed CM systems. (a) Detailed two-stage model investigated by simulation. (b) Simplified single-stage model for experimental testing.

III. CM Test Platform in PLECS Simulation

A. PLECS System Model

A PLECS model incorporating mechanical, electrical, and thermal behaviors is used to create a simulated test platform for the CM system. A model of the HKT mechanical system outputs rotor torque according to the water velocity and PMSG speed, considering the tip-speed ratio (TSR) and power coefficient (C_P) of the turbine. Next, a model of the PMSG determines the phase currents and voltages that should be applied by the gen-side converter. The converter features Microchip MSC040SMA120B 1200 V SiC MOSFETs with a nominal R_{dson} of 40 mΩ. In the PLECS simulation, the manufacturer's PLECS thermal model is used to model MOSFET power loss. The simulation includes the thermal circuit of Fig. 2, where h varies with river water velocity and temperature. For simplicity, a single half-bridge of the three-phase gen-side converter is considered in the test platform, without loss of generality. The electrical behaviors of the gen-side converter and PMSG are replicated by an H-bridge circuit with an inductive load as described in [9]. One of the H-bridge half-legs comprises the device-under-test (DUT) MOSFETs, which see the same load current and switching behavior as a single phase of the gen-side converter would see in controlling the PMSG.

B. Simulated CM System Training

The first step of the training is to collect a large dataset of measurements from the PLECS simulation, including all of the required ML model features (inputs) and targets (outputs), as shown in Fig. 3(a). The PLECS simulation is swept over water temperatures from 0 to 20°C in increments of 2.5°C, and over water speed from 0.9 to 4.65 m/s in increments of 0.25 m/s. Once each simulation reaches steady-state, 40 data samples are collected. The samples are taken at the PMSG fundamental frequency, and timed to coincide with the peak of the load current. This maximizes the signal-to-noise ratio of the drain-source voltage and drain current measurements. This generates a dataset with 6120 instances (feature and target sets). The dataset is then imported into the Python environment for training and testing of the ML models. A randomized 80% / 20 % split is used to divide the dataset into training and testing sets, respectively. In training, the known Q is given to ML Model 1, and the known R_{dson} value calculated from I_D and V_{ds} is given to ML Model 2. Whereas in testing, the models must predict Q and R_{dson}, and these predictions are compared to the known values to evaluate the performance of the models. Using this training and testing process, the models' hyperparameters such as the regularization weight or learning rate are tuned in order to maximize the performance of the models.

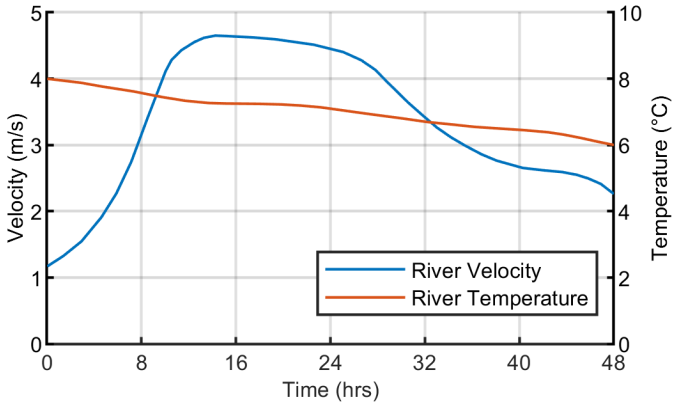

Fig. 4. Mission profile showing river speed and temperature over a 48-hour period.

C. Simulated Mission Profile Test

Now that the ML models have been trained over the expected operating conditions of the system, the CM system's performance during normal operation is investigated. In real deployment, the CM system with the ML models would be implemented in real-time. A 48-hour mission profile is considered with two test cases. In the first case, the HKT converter MOSFETs are in healthy BOL condition. In the second case, the MOSFETs have degraded such that their R_{dson} has increased by 10% compared to BOL R_{dson}. Fig. 4 shows the mission profile of river velocity and temperature. River velocity initially increases by 3.48 m/s before decreasing

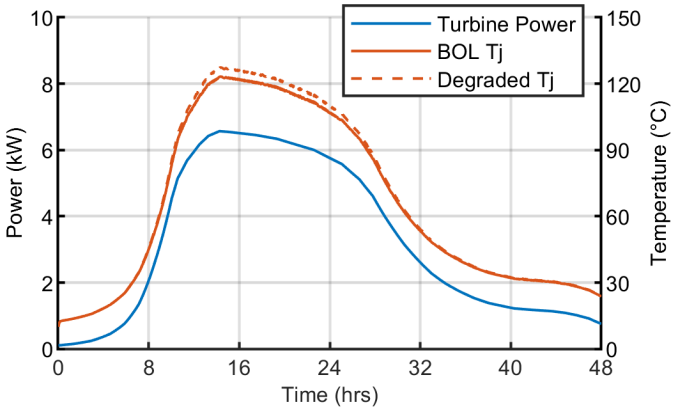

Fig. 5. Variation of HKT power and MOSFET junction temperature over the 48-hour mission profile.

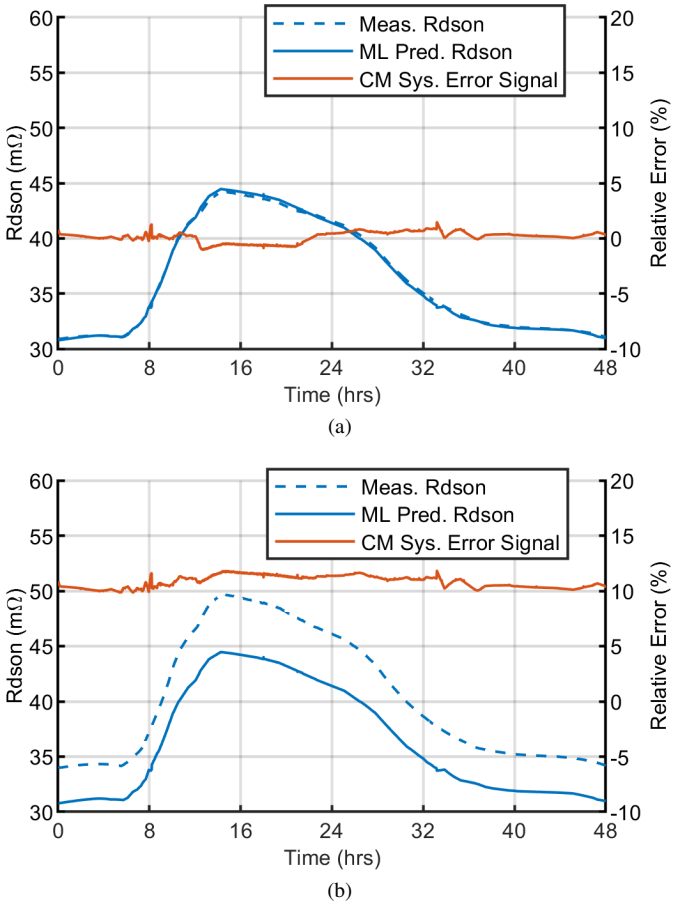

Fig. 6. Measured vs ML model predicted MOSFET R_{dson} (blue) and CM system error signal showing relative change from BOL R_{dson}. (a) MOSFET in BOL condition. (b) Degraded MOSFET.

gradually, whilst temperature drops by $2°C$ over the 48-hour period. Fig. 5 shows HKT system turbine power (PMSG input power) and converter MOSFET T_J for the two test cases. Turbine power is proportional to the cube of the water velocity, provided that optimal TSR is achieved where C_P is at its maximum. Therefore, the converter MOSFETs see a wide

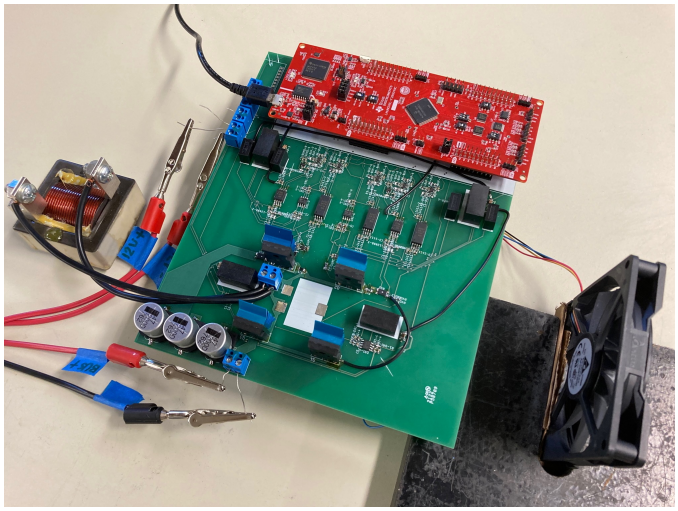

Fig. 7. Hardware test platform with fan, custom PCB with test circuit and measurement circuitry, MCU for controls and monitoring, and external load inductance.

variation in load currents and temperatures over the mission profile due to the HKT application.

Fig. 6 shows the performance of the proposed CM system for the two test cases: (a) converter MOSFETs in BOL condition; and (b) degraded converter MOSFETs where R_{dson} is 10% higher than BOL R_{dson}. Fig. 6(a) shows that for a BOL MOSFET, the ML model predicted R_{dson} closely tracks the actual measurement. The error signal has only minor variations from the expected value of 0 %. Fig. 6(b) shows for a degraded MOSFET, the predicted R_{dson} is consistently lower than the actual measurement. This is intended, since the ML model still predicts R_{dson} as though the MOSFET is in BOL condition. Indeed, the error signal successfully tracks the known % increase in R_{dson} of 10%. At around time = 14 hrs the error signal increases from 10% to around 12%, corresponding to the peak in T_J. While the simulation sets R_{dson} to be 10% higher at any given drain current and T_J, the increased resistance also causes increased conduction losses and therefore increased T_J. Since R_{dson} has a strong temperature dependence, the actual peak R_{dson} in the degraded MOSFET test case is 12.4% higher than in the healthy MOSFET test case.

IV. Experimental Testing

A. Experimental Test Platform Design

The test circuit simulated above is now implemented in hardware. The hardware test platform uses a custom PCB with control code deployed to a Texas Instruments F280049C development board. The hardware test also uses the Microchip MSC040SMA120B 1200 V SiC MOSFETs with a nominal R_{dson} of 40 mΩ. Fig. 7 shows the experimental test platform. Due to infrastructure limitation, the test platform is air-cooled rather than water-cooled. However, regardless of the cooling medium, the underlying physical mechanisms are the same.

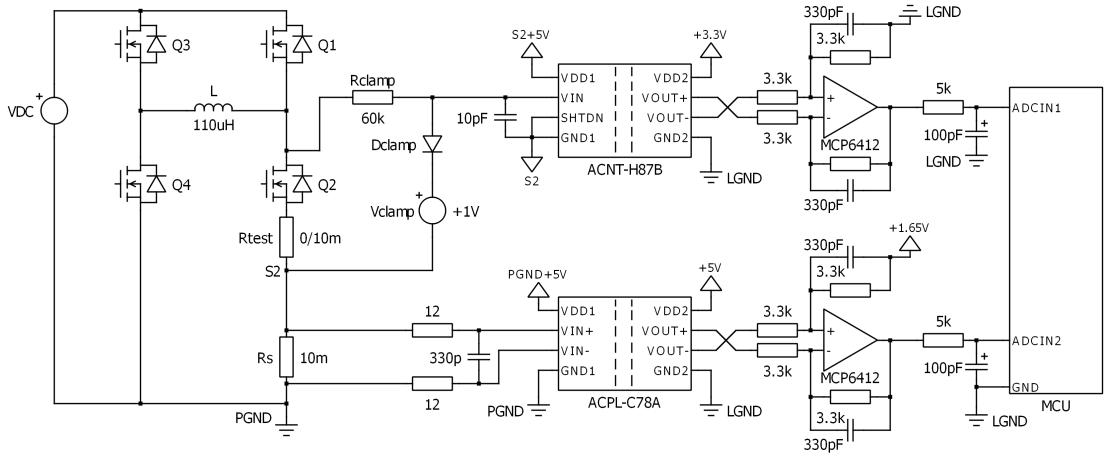

Fig. 8. Simplified schematic to show measurement circuitry for lower DUT SiC MOSFET (as implemented in Fig. 7 PCB).

There is conductive heat transfer between the MOSFET junction and the heatsink surface, and from the heatsink surface there is heat transfer to the water or air via forced convection. However, in the water cooled case, the convective heat transfer is many times more effective than in the air cooled case. In practice, this means the temperature difference between the heatsink and ambient will be far higher in the air-cooled case compared to the water-cooled case.

There are three major challenges in realizing the proposed CM system in hardware: Firstly, the measurements must be precise and temperature-independent due to the low R_{dson} of the SiC MOSFETs and high operating temperature range. Secondly, voltage clamping circuity is required to protect the sensitive low-voltage measurement circuitry from the DC bus voltage. Thirdly, the measurements must be sent across the isolation barrier between the high voltage power circuit and the low voltage logic circuits. Note that while the DC bus voltage in the hardware test is only 60 V, the use of isolated gate drivers and isolation amplifiers allows the proposed CM system to be implemented at much higher voltage levels.

Fig 8. shows a simplified schematic of the PCB measurement circuitry for the lower DUT MOSFET. Note that the equivalent measurement circuitry implemented for the upper DUT MOSFET is not shown. Additionally, gate drive, power supply, and other auxiliary circuitry are omitted. The proposed CM solution requires precise measurement of each DUT MOSFET's drain current and drain-source voltage. Therefore, kelvin connection shunt resistors with +-0.1% tolerance are used for drain current sensing. The current sense resistor voltage drops are amplified by Broadcom ACPL-C78A isolation amplifiers. An operational amplifier then converts the double-ended output signal into a single ended signal for connection to a microcontroller ADC. Low pass filters at the isolation amplifier and ADC inputs filter out high-frequency noise.

The drain-source voltage measurements use Broadcom ACNT-H87B isolation amplifiers. The voltage at the amplifier's VIN pin must not exceed 5 V relative to the GND1 pin. Therefore, a clamping circuit must be employed to block the DC bus voltage during the MOSFET's off-state. For example, when the lower MOSFET is off, the upper MOSFET is on, and therefore the lower MOSFET drain voltage is pulled to the DC bus voltage whilst the source is at ground. i.e. the DC bus voltage would appear across the amplifier inputs when the MOSFET is off. To prevent this, voltage clamping circuits using diodes, zener diodes or auxiliary MOSFETs are commonly used. However, these conventional current clamping circuits induce an error in the voltage measurement due to diode leakage currents. This problem is exacerbated by the strong temperature dependence of the leakage current, which leads to an increasing error at higher temperatures. To alleviate the leakage current issue, the authors of [10] propose a clamping circuit in which a voltage source is used in place of a zener diode. This circuit design is implemented here using a 60 kΩ clamp resistor, a schottkey diode, and a 1V source referenced to the MOSFET source. Here, the 1V source is implemented using an isolated switching converter. Similar to the current sensing circuitry, the double-ended output signal of the ACNT-H87B is converted to a single-ended signal before connection to the microcontroller ADC.

ADC measurements are trigged by the PWM generation, such that the lower MOSFET measurements are obtained during the midpoint of the lower MOSFET on-time, and the upper MOSFET measurements during the midpoint of the upper MOSFET on-time. Within the controller, these measurements are sampled a second time to obtain Vds_{pk} and Id_{pk} as the measurements corresponding to the peak of the load current sinusoid.

B. Experimental CM System Training

The experimental test platform considers scaled turbine and PMSG models to calculate reference load current magnitudes from the water velocity. Training data is gathered at a constant ambient temperature of around 20°C and a fundamental frequency of 15.9 Hz. Water velocity is swept from 1 to 2 m/s in increments of 0.1 m/s. At each water velocity and corresponding load current magnitude, 40 s of measurements

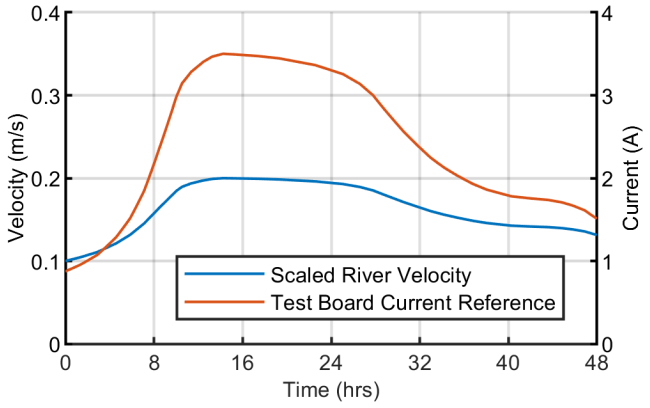

Fig. 9. Mission profile showing scaled river speed and reference load current magnitude for the hardware test.

are obtained. The microcontroller records measured drain-source voltages, drain currents, and the current space vector magnitude. This data is then used to train and test the ML model of Fig. 3(b), using the same process as described above for the Fig. 3(a) models. The ML model features are now the MOSFET drain current Id_{pk}, the current space vector magnitude Is_{mag}, and the water velocity V_{inf}. The ML model target is MOSFET R_{dson}, calculated as MOSFET drain-source voltage Vds_{pk} divided by Id_{pk}.

Note that Id_{pk} and Vds_{pk} are not raw measurements. The drain-source voltage and drain current measurements are obtained over the entire load current sinusoid. However, the controller takes one sample per fundamental frequency cycle at the moment where the load current through each MOSFET is at its maximum. Additionally, these controller sampled Vds and Id measurements are then averaged over 0.5 s to obtain Vds_{pk} and Id_{pk} for R_{dson} calculation and input to the ML model. In the experimental test, the averaging and ML model deployment are performed offline. In real application, these steps would be undertaken in real-time, either on the controller board or on a remote system.

As in the PLECS simulated test, the trained ML model will predict the R_{dson} of a MOSFET in its healthy BOL condition. The proposed CM system then compares the measured R_{dson} to this predicted R_{dson} to produce an error signal for R_{dson}. If the MOSFET is in healthy condition, the error signal should be approximately zero. However, when the MOSFET degrades and the measured R_{dson} increases, the error signal should reflect the increase in R_{dson} from the BOL R_{dson} value.

C. Experimental Mission Profile Test

The experimental CM system testing is performed in a similar manner to the above simulated testing. The mission profile of Fig. 9 is now applied to the hardware test platform. However, since ambient temperature was uncontrolled, the river temperature is not considered. The river velocity profile is also scaled to the minimum and maximum values of the experimental test platform, 0.1 and 0.2 m/s, respectively.

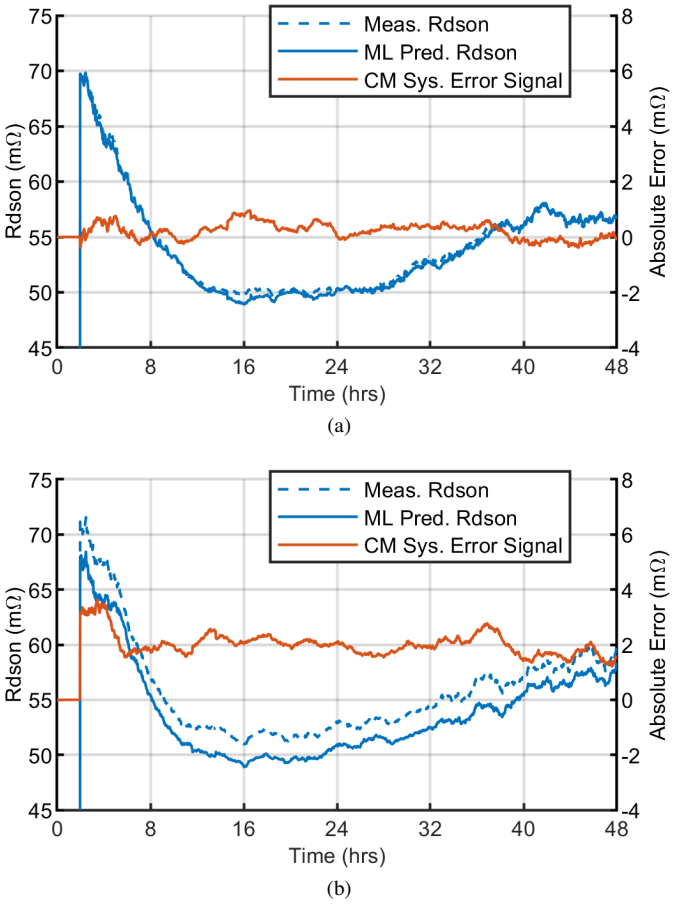

Fig. 10. Measured vs ML model predicted MOSFET R_{dson} (blue) and CM system error signal showing absolute change from BOL R_{dson}. (a) MOSFET in BOL condition. (b) Emulated degraded MOSFET.

This allows testing over the full range of expected operating conditions. The experimental test applies time scaling to the mission profile, such that it is completed 100x faster. i.e., the 48 hr mission corresponds to an actual test duration of 28.8 minutes.

As before, the mission profile is applied to two test cases. The first test case represents a HKT converter MOSFET in healthy BOL condition. In the experimental test platform, a healthy BOL MOSFET is used, and Rtest in Fig. 8 is a 0 Ω jumper. The second test case represents a degraded HKT converter MOSFET with increased R_{dson}. Here, the same healthy BOL MOSFET is used, but Rtest is replaced with a 10 mΩ resistor. Therefore, the drain-source voltage measurement circuit will measure R_{dson} as the MOSFET's BOL R_{dson} plus Rtest, emulating a degraded MOSFET for testing purposes. To improve the clarity of the results, 2-hr moving averages are shown for the calculated R_{dson}, ML model predicted R_{dson}, and the output error signal of the CM system. In real deployment, similar averaging can be applied to the CM system error signal to balance the responsiveness and noise rejection of the CM system.

Fig. 10. shows the performance of the experimental CM system for the two test cases. The dashed blue line shows the

measured R_{dson}, which is directly calculated from the Vds and Id hardware measurements. The solid blue line is the ML model's predicted R_{dson}. Recall that since the ML model is trained only with healthy MOSFET data, the ML model always predicts R_{dson} for a healthy MOSFET, regardless of the actual MOSFET condition. The orange line is then the absolute difference between the measured and predicted R_{dson} values, obtained as shown in Fig. 3(b). In contrast to the simulated tests, the measured R_{dson} actually reduces with increasing load. This does not reflect the expected behavior, and can likely be attributed to errors in the measurement circuits. However, a benefit of the ML approach is that the ML model adapts to the experienced behaviors, since the ML model is trained on the same circuit with the same errors present.

Fig. 10(a) shows the test with a healthy BOL condition MOSFET. In this case, the predicted R_{dson} should match the measured R_{dson}, and the absolute error signal should be zero. Although some noise is present on the error signal, it remains close to zero within ± 1 mΩ over the full mission profile load variation. Fig. 10(b) shows the test with the emulated degraded MOSFET. In this case, the measured R_{dson} signal should be 10 mΩ higher than the predicted R_{dson} across the entire mission. However, the absolute error signal tracks a difference of only around 2 mΩ.

Comparing between the error signals for the healthy and degraded MOSFETs, the CM system is clearly capable of drawing a distinction between the a healthy and degraded MOSFET. However, the absolute accuracy of the system is still lacking. This suggests the measurement circuitry is not functioning as well as anticipated, and is not accurately measuring the drain-source voltage or drain current. Despite this, the ML based CM system shows promise for SiC MOSFET degradation monitoring via an increase in drain-source resistance. Future experimental testing should attempt to increase the accuracy of the measurement circuitry, as well as testing a more complex ML model which also considers the ambient temperature.

V. Conclusion

This work proposes a ML based SiC MOSFET CM system, especially for the HKT application. To account for MOSFET R_{dson} load and temperature dependencies, supervised training is used across the entire operating space. Through this process, changes in MOSFET T_J due to varying power loss, river temperature, and the convective heat transfer coefficient under changing river velocity are all compensated for in the prediction of R_{dson}. The ML models are trained exclusively with MOSFETs in the BOL condition, while the real R_{dson} measurement will include any increase in resistance due to intrinsic or extrinsic degradation mechanisms, including dielectric breakdown. This allows the proposed CM system to use the difference between predicted and measured R_{dson} to track degradation independently of I_D and T_J. Compared to existing methods, this removes the need to explicitly measure or estimate MOSFET T_J via a case temperature measurement or MOSFET TSEP. An additional advantage is that neither MOSFET power loss nor the complex HKT system cooling behaviors need to be modeled.

The proposed ML models were successfully demonstrated using a 48-hour mission profile case study in which the river velocity sees a wide variation. In the simulated tests, despite a change in junction temperature of over $100°C$ in the mission profile, the known % change in MOSFET R_{dson} was successfully tracked in healthy and degraded test cases. In the hardware testing, the performance of the CM system was degraded compared to the simulated tests. However, the CM system was still able to identify a clear increase in R_{dson} over the mission profile.

The proposed CM system offers tangible benefits to HKT systems, which often suffer from higher operational costs compared to other renewable systems such as wind turbines. When combined with accelerated life testing data, the CM system can enable remaining useful life prediction or failure prognosis. These techniques can support condition based maintenance, in which the HKT system is serviced according to the system's current condition. HKT system availability is improved since MOSFET failures and the associated system downtime can be avoided. Reduced operational costs and increased availability contribute to a reduction in the levelized cost of energy of the HKT system, improving its commercial viability. The proposed method is suitable for deployment in many other applications, and the structure of the ML models can be adapted to suit the available measurements and requirements of each system.

References

[1] S. Pu, F. Yang, B. Vankayalapati, and B. Akin, "Aging Mechanisms and Accelerated Lifetime Tests for SiC MOSFETs: An Overview," *IEEE Trans. Emerg. Sel. Topics Power Electron.*, pp. 1–1, 2021.

[2] R. Wu, F. Blaabjerg, H. Wang, M. Liserre, and F. Iannuzzo, "Catastrophic failure and fault-tolerant design of IGBT power electronic converters - an overview," in *Proc. 39th Annu. Conf. IEEE Ind. Electron. Soc.*, Nov. 2013, pp. 507–513.

[3] E. Ugur, F. Yang, S. Pu, S. Zhao, and B. Akin, "Degradation Assessment and Precursor Identification for SiC MOSFETs Under High Temp Cycling," *IEEE Trans. Ind. Appl.*, vol. 55, no. 3, pp. 2858–2867, May 2019.

[4] F. Erturk, E. Ugur, J. Olson, and B. Akin, "Real-Time Aging Detection of SiC MOSFETs," *IEEE Trans. Ind. Appl.*, vol. 55, no. 1, pp. 600–609, Jan. 2019.

[5] F. Yang, S. Pu, C. Xu, and B. Akin, "Turn-on Delay Based Real-Time Junction Temperature Measurement for SiC MOSFETs With Aging Compensation," *IEEE Trans. Power Electron.*, vol. 36, no. 2, pp. 1280–1294, Feb. 2021.

[6] C. M. Bishop, *Pattern Recognition and Machine Learning*. New York, NY: Springer, 2006, ch. 3.

[7] ——, *Pattern Recognition and Machine Learning*. New York, NY: Springer, 2006, ch. 5.

[8] D. P. Kingma and J. Ba, "Adam: A method for stochastic optimization," *arXiv preprint arXiv:1412.6980*, 2014.

[9] U.-M. Choi, F. Blaabjerg, and S. Jørgensen, "Power Cycling Test Methods for Reliability Assessment of Power Device Modules in Respect to Temperature Stress," *IEEE Trans. Power Electron.*, vol. 33, no. 3, pp. 2531–2551, Mar. 2018.

[10] B. Yu, L. Wang, and D. Ahmed, "Drain–Source Voltage Clamp Circuit for Online Accurate ON-State Resistance Measurement of SiC MOSFETs in DC Solid-State Power Controller," *IEEE Trans. Emerg. Sel. Topics Power Electron.*, vol. 8, no. 1, pp. 331–342, Mar. 2020.